

NanoInclusions in Dry Polymer Brushes

Jaeup U. Kim

Department of Chemical Engineering, Columbia University, 500 West 120th Street,
New York, New York 10027

Ben O'Shaughnessy*

Department of Chemical Engineering, Columbia University, 500 West 120th Street,
New York, New York 10027

Received April 18, 2005; Revised Manuscript Received October 19, 2005

ABSTRACT: A theory of dry polymer brushes containing nanoInclusions is presented. Polymer brush–nanoparticle mixtures arise in various applications and in experimental systems where block copolymer materials, providing brushlike environments, organize nanoparticles to generate materials with novel properties. The ease with which a nanoInclusion enters a brush is measured by the free energy cost to introduce the inclusion, ΔF^{inc} . This depends strongly on particle shape and size b , as does the degree to which brush chain configurations are perturbed. For inclusions smaller than the typical chain fluctuation scale or blob size ξ_{blob} , by extending the self-consistent mean field (SCF) theory for pure brushes, we show $\Delta F^{\text{inc}} = P(z)V_p$ for an inclusion of volume V_p a distance z from the grafting surface. Here $P(z)$ is the quadratic SCF “pressure” field. Equilibrium particle distributions within a brush of chains of length N grafted at density σ depend strongly on particle size: (i) particles smaller than a scale $b^* \sim \sigma^{-2/3}$ distribute uniformly, dominated by entropy, while (ii) larger inclusions penetrate the soft surface region of the brush in a layer of thickness $\delta \approx h(b^*/b)^3$ where h is brush height and (iii) complete expulsion occurs for sizes above $b_{\text{max}} \sim (N/\sigma)^{1/4}$. Inclusions bigger than ξ_{blob} affect chain configurations much more strongly and require a different theoretical approach. We show $\Delta F^{\text{inc}} = \beta P(z)V_p$, where β is a shape-dependent constant for which we obtain rigorous bounds. Vertically oriented cylinders achieve the minimum energy cost ($\beta = 1$). Motivated by exact results for the approximate Alexander–de Gennes brush (chain ends fixed at brush surface), we argue that disk-shaped inclusions incur maximum energy cost ($\beta \sim t$ where t is the disk aspect ratio).

I. Introduction

Much experimental and theoretical research has focused on the basic principles governing polymer brushes, assemblies of chains end-grafted to a surface. Our goal in this paper is to understand the behavior of nanosized *inclusions* in brushes (Figure 1): how are nanoInclusions spatially distributed, and how readily will a brush accommodate them? How do the inclusions influence the host brush, and what brush free energy changes do they generate? How does all of this depend on nanoInclusion size? While theory for pure brushes and related block copolymer systems is very well developed,^{1–7} the behavior of these composite systems is relatively unexplored.^{8–14}

We are motivated to study these systems because, on one hand, brushlike systems frequently carry particle impurities, while impurities intentionally introduced into brushes can enhance physical properties and create materials with novel properties. These depend not only on the properties of the inclusions themselves but also on their spatial arrangements; indeed, organizing nanocomponents into complex spatial superstructures is a major challenge in nanoscience and nanotechnology. The technological potential lies in novel magnetic, electric, and optical properties. A recent nanoInclusion–brush study indicates that inhomogeneously grafted polymers can control nanoparticle distributions,^{15,16} with potential applications for nanoparticle-based catalysts and sensors.

Understanding how protein nanoInclusions can penetrate grafted polymer layers is another important application; this is

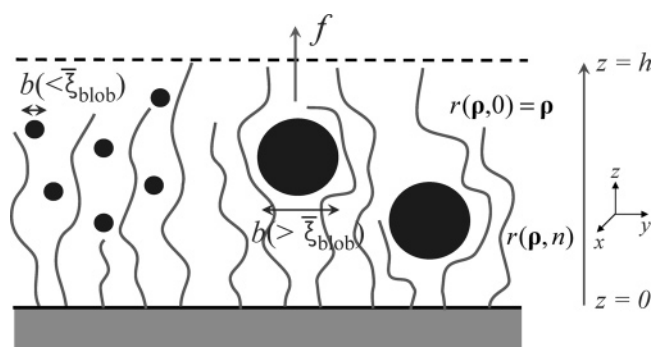


Figure 1. Polymer brush containing nanoInclusions of various sizes. $\mathbf{r}(\mathbf{p},n)$ is the position of the n th monomer of a chain whose end lies at \mathbf{p} . Inclusions smaller than the brush blob size ξ_{blob} do not significantly interfere with the path of a chain, while larger inclusions induce strong lateral (x, y) stretch. Because of the gradient in stretching energy penalty, inclusions experience effective buoyancy forces strongly depending on inclusion shape and volume V_p .

important in bioengineering approaches to preventing surface-induced thrombosis in blood-contacting materials by using polymer-coated surfaces to inhibit protein binding.^{17–20} Here the nanoInclusions can range from single proteins to aggregated protein particles of various sizes and shapes. The interaction of proteins with wet brushes has been studied theoretically.^{17,19,20} In ref 19 enthalpic interaction and kinetic barriers were the major source of protein–brush repulsion. Halperin¹⁷ found shape-dependent protein–brush interactions originating from van der Waals interactions between the proteins and the grafting surface.

Another motivation is to better understand nanoInclusions in block copolymer hosts, for which brushes provide a first model.

* To whom correspondence should be addressed. E-mail: bo8@columbia.edu.

The physics of brushes is closely related to block copolymer behavior;¹ each layer in a lamellar phase is a brush, albeit with annealed grafting density, while phases with cylindrical and spherical geometry are closely related to brushes grafted on curved surfaces.²¹ Periodic structures provided by block copolymer materials can act as templates to arrange nanoinclusions. For example, by localizing metal nanoparticles in lamellar phases, composite inorganic–organic materials have been created with novel optical filtering properties.^{22–24} The advantage of such approaches is that particle organization happens naturally and thermodynamically, promising rapid and inexpensive manufacture of nanostructured composite materials.

The theory of brushes is well developed. At high enough surface grafting density σ , chains are forced to stretch due to lateral excluded-volume interactions with one another. Because of stretch, brush height h is proportional to the number of monomer units per polymer, N . Our interest here is confined to dry brushes (no solvent),^{1,2} though many concepts from wet brushes^{6,7} are in common.

Our starting point is the self-consistent mean field (SCF) theory of Semenov,^{1,2} who showed that the self-consistent “pressure” field $P(z)$ for a molten brush has quadratic form:

$$P(z) = P_0 \left(1 - \frac{z^2}{h^2} \right); \quad P_0 \equiv 3\pi^2 h^2 / 8N^2 a^5; \quad g(\rho) = \frac{\sigma}{h} \frac{\rho}{\sqrt{h^2 - \rho^2}} \quad (1)$$

This field $P(z)$ represents the effect of all the other chains on a given chain; it is a Lagrange multiplier enforcing constant density. To satisfy constant density, the free chain ends must follow the distribution $g(\rho)$ where ρ is the free end location. Note the variables z and ρ have values between 0 and h (see Figure 1). The brush height h is $\sigma N a^3$, where a is the monomer size. The pressure field at the grafting surface, $z = 0$, is P_0 (we choose units where $k_B T$ is unity). An essential feature of Semenov’s theory is that chain ends are distributed everywhere throughout the brush, in contrast with the simplified Alexander–de Gennes approximation^{3–5} which assumes that all chain ends are constrained to be at the free brush surface, $z = h$.

By extending Semenov’s method, we will develop a theoretical analysis of brush–nanoinclusion mixtures. The present work is entirely concerned with brushes in the strongly stretched limit of the Semenov theory, i.e., $h \gg R_G$ where R_G is the unperturbed chain size (corrections for moderately stretched brushes are beyond the scope of this work^{25,26}). For a small inclusion of volume V_p at height z in the brush, we will show that the brush free energy change, ΔF^{inc} , equals $P(z)V_p$. It follows that nanoinclusions smaller than a certain scale b^* mix readily into the brush, while larger inclusions are forced near the free brush surface where $P(z)$ is small; i.e., the brush is soft enough to host them. Thus, there is a “buoyancy” effect tending to push relatively large nanoinclusions to the top surface.

For inclusions which are so large that a given chain trajectory is forced to deviate strongly in the lateral directions (x, y in Figure 1) the story is much more complex. This happens when particle size exceeds a characteristic fluctuation scale of a chain in the particle-free brush, ξ_{blob} . For such particles, we use an analogy connecting our polymer problem to a hydrodynamical system to show that for sphere and cylinder shapes $\Delta F^{\text{inc}} \approx P_A V_p$, where P_A is a characteristic pressure, while for disks the effective volume is that of a sphere. This hydrodynamic analogy, however, describes only the approximate Alexander–de Gennes brush. When end-annealing is considered, we are able to prove

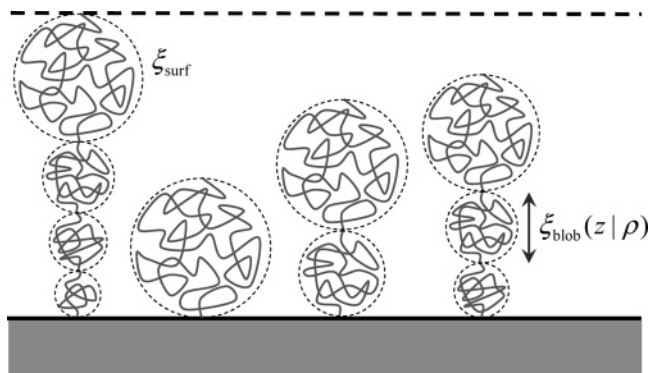


Figure 2. Chains in a polymer brush are stretched toward the free surface on average. Entropy produces fluctuations about the average path. The scale of these fluctuations, the blob size $\xi_{\text{blob}}(z|\rho)$, is an increasing function of z and depends also on the location of the chain end, ρ . The blob size at the brush surface is ξ_{surf} .

that $P(z)V_p$ remains the energy penalty to within prefactors of order unity for most shapes. For disks we obtain rigorous bounds.

The outline of the paper is as follows. In section II we briefly review polymer configurations in pure brush systems. We categorize brush–inclusion mixtures into two cases by comparing inclusion size b to the mean brush blob size ξ_{blob} . In section III we establish a formal framework for mixed brush–inclusion systems; the brush height change and chain end distribution due to inclusions are discussed. In section IV we show the brush free energy penalty due to small ($b < \xi_{\text{blob}}$) inclusions is $P(z)V_p$, enabling the equilibrium nanoinclusion distribution to be determined as a function of polymer size N and inclusion size b in section V. In section VI the brush free energy penalty due to larger ($b > \xi_{\text{blob}}$) inclusions is calculated, using the hydrodynamic analogy which applies to the Alexander–de Gennes brush. We show the brush response strongly depends on inclusion size. In section VII the proper end-annealed brush is considered; we determine upper and lower bounds for the brush free energy change due to incorporation of one inclusion. For most shapes, the shape-dependent energy penalty remains of order $P(z)V_p$. In section VIII we conclude with a brief discussion, and we compare our theory to experiment.

II. Brief Review of Dry Brush Theory

In this section we briefly review what has been established theoretically about nanoparticle-free brushes; this will be the starting point for our analysis. Grafted polymers at high surface coverage become stretched away from the grafting surface (see Figure 2). For a polymer whose free end lies a distance ρ from the grafting surface, we denote the distance of its n th monomer from the free end as $z(\rho, n)$. The incompressibility of the dry polymer brush creates a pressure field $P(z)$, which causes chains to stretch.^{2,27} In previous theoretical works, it was shown that^{1,6} the pressure field $P(z)$ contributes to the single chain free energy as follows (see section III):

$$F^{\text{chain}} = \int_0^N dn \left[\frac{3}{2a^2} \left(\frac{\partial z(\rho, n)}{\partial n} \right)^2 + P(z(\rho, n))a^3 \right] \quad (2)$$

To obtain the complete brush configuration, the sum of all the single chain free energies must be minimized, subject to the volume constraint. The full solution to this problem was obtained in Semenov’s SCF theory of ref 1, including the quadratic pressure field $P(z)$ and the chain end distribution $g(\rho)$ given by eq 1. (In section III and Appendix A, the derivation of $g(\rho)$ is

briefly outlined for completeness.) In ref 6 it was pointed out that the path of a chain in the pressure field $P(z)$ is related to the classical motion of a particle with mass $m = 3/a^5$ in the potential field $-P(z)$. In this analogy, the “stretch” of a chain, $\partial z/\partial n$, corresponds to the velocity of the particle; hence, an equation analogous to the conservation of kinetic plus potential energy relates $\partial z/\partial n$ to the pressure field:

$$\frac{3}{2a^5} \left(\frac{\partial z(\rho, n)}{\partial n} \right)^2 = P(z) - P(\rho) = \frac{3\pi^2}{8N^2 a^5} (\rho^2 - z^2) \quad (3)$$

Combined with the chain end distribution in eq 1, this chain path equation completes the full brush configuration. The SCF solution, however, is valid in the strongly stretched limit and provides only the average path of a chain, a straight path orthogonal to the grafting surface. The actual polymer path fluctuates about this average path on short length scales, ξ_{blob} . This is the blob size. As we will see, this scale defines the boundary between small and large inclusions.

Now since the pressure field $P(z)$ is a function of position in the brush z , the blob size ξ_{blob} also depends on z . Moreover, each chain has its own end position ρ , so the blob sizes of different chains at a given location z are in general different (see Figure 2). Let us define $\xi_{\text{blob}}(z|\rho)$ to be the blob size at z for a polymer with its free end at ρ . Denoting n_{blob} as the number of monomers in the blob, $\xi_{\text{blob}}(z|\rho) = n_{\text{blob}}^{1/2} a$ because below the fluctuation length scale monomers random walk. On the other hand, the SCF solution suggests a linear displacement $\simeq (\partial z/\partial n) n_{\text{blob}}$. The crossover from random walk statistics to the SCF solution defines the blob scale:

$$n_{\text{blob}}^{1/2} a \simeq \frac{\partial z}{\partial n} n_{\text{blob}} \quad (4)$$

Thus, $n_{\text{blob}}^{1/2} \simeq a/(\partial z/\partial n)$. Using eq 3, we have

$$\xi_{\text{blob}}(z|\rho) \simeq \frac{2Na^2}{\pi(\rho^2 - z^2)^{1/2}} \quad (5)$$

Note ξ_{blob} is a function of both ρ and z , so at location z many chains with different end positions $\rho > z$ coexist, each with its own blob size. Using the chain end distribution function $g(\rho)$, we now calculate the average blob size at z from eq 5, giving

$$\bar{\xi}_{\text{blob}}(z) \simeq \frac{Na^2}{\sqrt{h^2 - z^2}} \quad (6)$$

For most locations z in the brush we have $h - z = O(h)$, and thus in eq 6 the denominator approximates $h^2 - z^2 \simeq h^2$. Thus, the “typical” average blob size within the brush is given by

$$\bar{\xi}_{\text{blob}} \simeq Na^2/h \simeq \frac{1}{\sigma a} \quad (7)$$

This scale is simply the blob size of the simplified Alexander–de Gennes theory.^{3–5} For a given position z , those few chains which have ends ρ just above z have blobs larger than the above estimate; however, these contribute negligibly to the average blob size due to their rarity. In this study, we will use $\bar{\xi}_{\text{blob}}$ as the characteristic local chain fluctuation scale, since most chains have a blob size of this order.

The surface blob at $z = h$ is a special case. The z -dependent blob expression, eq 6, does not correctly describe its size, ξ_{surf} (it diverges unphysically as z approaches h). However, we can estimate ξ_{surf} using a simple argument related to that used to

analyze the penetration of chains into a brush surface in ref 28. From eq 1 the pressure field $P(z)$ near the free surface is approximately linear, $2P_0(h - z)/h$; hence, the mean pressure field acting on the monomers in the surface blob is $P_0 \xi_{\text{surf}}/h$. The blob size is obtained by equating the energy due to pressure, $n_{\text{blob}} a^3 \times P_0 \xi_{\text{surf}}/h$, to $k_B T$. Here $n_{\text{blob}}^{1/2} a = \xi_{\text{surf}}$ from random walk statistics. Thus

$$\xi_{\text{surf}} \simeq \left(\frac{8Na}{3\pi^2 \sigma} \right)^{1/3} \quad (8)$$

An important observation is that the surface blob size ξ_{surf} is much larger than that in the interior of the brush, $\bar{\xi}_{\text{blob}}$, reflecting the fact that the brush is much softer at the top surface than deep in its interior. In section V we will discuss how this soft surface region can hold nanoinclusions more easily than the interior of a brush.

III. Nanoinclusions in a Polymer Brush: Formal Framework

In this section the SCF theory is generalized to a brush containing nanoinclusions. This generalization shares some features of prior theoretical analyses of homopolymers in block copolymer systems.^{29–33} Consider a brush of chains grafted on a surface at $z = 0$ (see Figure 1) containing nanoinclusions distributed with some position-dependent volume fraction $\phi(\mathbf{r})$. We write the position of the n th monomer of a chain as $\mathbf{r}(\rho, n)$ where ρ is the position of the free end. In the strongly stretched regime, the total free energy is

$$F^{\text{brush}} = \int d\rho g(\rho) \int_0^N dn \frac{3}{2a^2} \left(\frac{\partial \mathbf{r}(\rho, n)}{\partial n} \right)^2 + \int d\mathbf{r}_\perp \eta(\mathbf{r}_\perp) \times (\sigma - \int d\rho g(\rho) \delta(\mathbf{r}_\perp(\rho, N) - \mathbf{r}_\perp)) - \int d\mathbf{r}' P(\mathbf{r}') a^3 \times \left(\frac{1}{a^3} (1 - \phi(\mathbf{r}')) - \int d\rho g(\rho) \int_0^N dn \delta(\mathbf{r}' - \mathbf{r}(\rho, n)) \right) \quad (9)$$

The first term is the total chain stretching energy at a given chain end distribution $g(\rho)$. The second term represents the constraint that chain end grafting density of this brush is σ . The transverse vector \mathbf{r}_\perp only has x and y components, and the Lagrange multiplier $\eta(\mathbf{r}_\perp)$ is the chemical potential of a chain (see Appendix B). The last term is from the condition that monomers plus nanoinclusions are space-filling; i.e., the monomer volume fraction is equal to $1 - \phi(\mathbf{r})$. The Lagrange multiplier imposing the density constraint is the pressure field $P(\mathbf{r})$, the 3-dimensional generalization of the 1-dimensional field $P(z)$.

The set of chain paths provides complete information about how polymers behave, given the nanoinclusion distribution $\phi(\mathbf{r})$. In the mean field framework, each chain selects its path to minimize its stretching energy under the given constraints; the chain path equation is obtained by minimizing F^{brush} with respect to $\mathbf{r}(\rho, n)$:

$$\frac{3}{a^5} \frac{\partial^2 \mathbf{r}(\rho, n)}{\partial n^2} = \nabla P(\mathbf{r}) \quad (10)$$

Note this chain path equation is in fact the same equation as that for pure brushes;^{1,6} even though the inclusion density field $\phi(\mathbf{r})$ modifies the pressure field $P(\mathbf{r})$, the chain path “dynamics” have no explicit dependence on $\phi(\mathbf{r})$.^{9,10} That is, chains and inclusions interact only through the pressure field $P(\mathbf{r})$.

Before solving the complete chain paths, we must know how the pressure field $P(\mathbf{r})$ changes at the given inclusion density

field $\phi(\mathbf{r})$. The general solution for the nonsymmetric 3D pressure field $P(\mathbf{r})$ that forces all chains to reach the grafting surface after N steps is rather difficult to find analytically. In fact, since inclusions represent singular domains, standard perturbative approaches are not valid, a point which we discuss briefly in section VI.

Our approach is nonperturbative. We treat a collection of small nanoinclusions as a fluidlike presence in the brush which occupies only a certain fraction of the available space; thus, the nanoinclusion fraction function $\phi(\mathbf{r})$ is smeared out, coarse-grained over the interparticle separation. Much of our interest will be in the *equilibrium* situation, where nanoinclusions have found their thermodynamically desired distributions. In equilibrium, symmetry dictates that the coarse-grained continuous nanoinclusion density field has no dependence in the directions parallel to the grafting surface. Thus, $\phi(\mathbf{r})$ depends only on the z coordinate (see Figure 1), and in consequence all other variables in the free energy also depend on z only. This is a considerable simplification.

The "fluidization" method ignores chain stretch in the lateral (x and y) directions, a good approximation for inclusions smaller than the fluctuation length scale ξ_{blob} , since then the lateral deviation enforced by an inclusion is less than the chain's intrinsic lateral fluctuation scale. In this and the following section we consider only this case. Inclusions larger than ξ_{blob} are considered in section VI and subsequent sections.

Specializing to such small inclusions, the full brush free energy, eq 9, now simplifies since all variables depend on z alone. (The simplified free energy is presented in Appendix B.) The dynamics, eq 10, are now one-dimensional, allowing the pressure field to be obtained analytically.

To satisfy the condition that every chain reaches the grafting surface after N steps, the 1D pressure field $P(z)$ must have the quadratic form displayed in eq 1,² where the brush height h is now increased by nanoinclusions relative to the inclusion-free brush value, h_0 . Volume conservation leads to

$$h = \frac{h_0}{(1 - \bar{\phi})}, \quad \bar{\phi} \equiv \int_0^h dz \phi(z)/h \quad (11)$$

Here $\bar{\phi}$ is the overall nanoparticle fraction. Given $P(z)$, one can now determine the chain end distribution $g(\rho)$ for an arbitrary nanoinclusion density distribution $\phi(z)$:

$$g(\rho) = \frac{\rho}{Na^3} \left(\frac{1 - \phi(h)}{\sqrt{h^2 - \rho^2}} + \int_\rho^h dz \frac{d\phi(z)/dz}{\sqrt{z^2 - \rho^2}} \right) \quad (12)$$

The method is presented in ref 10. In Appendix A this result is obtained in a rather simple way.

Note that the quadratic pressure field $P(z)$ was calculated under the assumption that chain ends occupy all locations $0 < \rho < h$. Now if eq 12 then gives negative $g(\rho)$ in any domain, this indicates $P(z)$ is wrong. It must then be recalculated under the constraint of chain-end-free zones.²¹ Interestingly, eq 12 implies that as long as $\phi(z)$ is an increasing function of height z , the function $g(\rho)$ is guaranteed positive. In section V, we show $\phi(z)$ must indeed always be monotonically increasing to satisfy conditions of thermodynamic equilibrium. Hence, the quadratic pressure profile and the chain end distribution of eqs 1 and 12 are valid when nanoinclusions have reached equilibrium within the brush.

IV. Chain Stretching Energy Penalty Due to Inclusions

To obtain equilibrium nanoinclusion density distributions, the change in the brush free energy ΔF^{inc} due to inclusions must

be determined and then minimized. In this section we obtain ΔF^{inc} for a given profile $\phi(z)$.

Knowing $P(z)$ and $g(\rho)$, the total chain stretching energy per unit area can be calculated. This is the sum of all individual chain stretching energies:

$$F^{\text{stretch}} = \int_0^h d\rho g(\rho) \int_0^N dn \left(\frac{\partial z(\rho, n)}{\partial n} \right)^2 \quad (13)$$

Since $g(\rho)$ is quite complex (see eq 12), it is rather difficult to evaluate this integral directly. It can be calculated, however, in a similar way to that used for pure brushes.^{29–33} Although the stretching energy of each polymer chain depends on the location of its free end, the sum of its stretching plus pressure energies (eq 2) is a constant, regardless of chain end position. Thus, the stretching energy can be expressed in terms of the pressure field $P(z)$ and the inclusion fraction $\phi(z)$, without explicitly involving $g(\rho)$. One then finds

$$F^{\text{stretch}} = \int_0^h dz (P_0 - P(z))(1 - \phi(z)) \quad (14)$$

A detailed derivation is presented in Appendix B.

For any given nanoinclusion distribution $\phi(z)$, eq 14 provides the exact chain stretching energy. If the mean nanoinclusion density $\bar{\phi}$ is small, this can be further simplified (see Appendix B):

$$\Delta F^{\text{inc}} = \int_0^h dz P(z)\phi(z) + O(\bar{\phi}^2) \quad (15)$$

This result tells us that inserting an inclusion at a height z generates energy penalty $P(z)V_p$. Since the pressure decreases with height z , an inclusion experiences an upward buoyancy force rather analogously to a macroscopic object in water. Note that the meaning of $P(z)$ is the pressure relative to that at the brush surface (we chose $P(h) = 0$).

Note that $P(z)V_p$ is the free energy of an inclusion located at z relative to the free energy it would have at location $z = h$. Thus, ΔF^{inc} is the free energy of the inclusion profile $\phi(z)$ relative to the free energy of the same inclusions were they all located at $z = h$ ($\phi(z) = \delta(z - h)\bar{\phi}h$). Thus, ΔF^{inc} describes how particles tend to distribute within the brush, given they are inside the brush. Thus, polymer–particle enthalpic interactions provide an additive constant to the total energy and can be ignored.

V. Equilibrium Nanoinclusion Distribution

Equations 14 and 15 give the free energy cost for a general inclusion density distribution $\phi(z)$. In typical experiments, however, $\phi(z)$ is not directly controllable. In this section we calculate the distribution assuming kinetics permit equilibrium to be reached.

Consider nanospheres of radius b and volume V_p at small volume fraction such that the chain stretching free energy of eq 15 applies. Adding a simple Flory–Huggins particle entropy term, the total free energy change per unit area is

$$\Delta F^{\text{total}} = \int_0^h dz P(z)\phi(z) + \int_0^h dz \frac{\phi(z)}{V_p} \log \phi(z) + \mu \left(h\bar{\phi} - \int_0^h dz \phi(z) \right) \quad (16)$$

Higher-order terms in $\phi(z)$ representing interparticle interactions were neglected for consistency with eq 15. The last term,

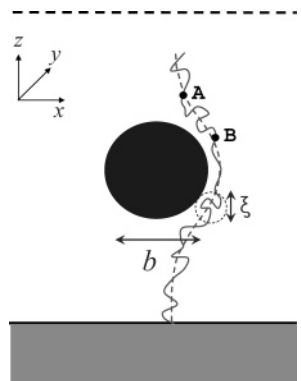


Figure 5. Chain path near a large inclusion ($b > \bar{\xi}_{\text{blob}}$) is significantly altered. This implies the local pressure difference between typical locations A and B, ΔP_{AB} , has a value of order the unperturbed pressure $P(z)$.

A. Lateral Stretch Is a Large Perturbation. Consider a chain passing near an inclusion whose free end is far removed from the inclusion. The difference in pressure ΔP_{AB} between two locations A and B belonging to a chain trajectory can be estimated as follows (see Figure 5).

During its journey from A to B, the direction of this polymer path is significantly tilted; i.e., the chain stretch $\mathbf{u} \equiv \partial \mathbf{r} / \partial n$ gains an x direction component u_x of order u_z . Since the distance between the points is of order b in both z and x directions, the number of monomers Δn between A and B is given approximately by $u_z \Delta n \approx b$. Estimating the x directional stretch change from the chain path equation, eq 10, we have $u_x \approx a^5 (\partial P / \partial x) \Delta n \approx a^5 (\partial P / \partial x) b / u_z$, and thus

$$\Delta P_{AB} \approx (\partial P / \partial x) b \approx u_z^2 / a^5 \approx P(z) \quad (22)$$

where the last identity in eq 22 follows from eq 3. Thus, near a large inclusion the pressure change is *comparable to the unperturbed pressure*. This is a simple but important conclusion.

It follows that perturbation theory,^{9,10} which assumes the relative change in pressure and other variables is much less than unity, cannot describe large nanoparticles. An appropriate description must yield a pressure field with short scale features near such a large inclusion.

Note that the above argument (leading to eq 22) also tells us that it is now essential to include lateral displacements of chain trajectories because these induce order unity pressure changes. Our fluidization approach for small nanoparticles neglects lateral displacements and must therefore be replaced by another approach. It is tempting to argue that a perturbative approach may work for particles much smaller than the brush size, $b \ll h$, even if they are large in the sense $b > \bar{\xi}_{\text{blob}}$. This is wrong, however: since the pressure perturbation due to lateral deviations is order $P(z)$, thus the corresponding free energy change is order $P(z)V_p$. This is of the same order as the free energy result in the fluidization approach of section IV. In the next subsection, we use an entirely different approach.

B. Chain Path around a Single Large Inclusion: Hydrodynamic Analogy. Our initial goal is to find the chain configuration $\mathbf{r}(\rho, n)$ and the pressure field $P(\mathbf{r})$ around a large

nanoinclusion of arbitrary shape. To our knowledge, no analytical theory has to date produced complete solutions, and the major tools in past work have been numerical methods.^{11–14}

Our starting point is an interesting analogy identified by Pincus and Williams³⁴ between a brush containing inclusions and a certain hydrodynamic problem. The analogy in fact only applies to the approximate Alexander–de Gennes (AG) brush whose ends are assumed all to lie at the brush surface. For this subsection and the next, we use this approach to determine chain paths and brush free energies. The results and concepts will prove very helpful in understanding the true end-annealed brush, which is considered in section VII.

The observation of Pincus and Williams is that the paths of polymer chains in a brush–inclusion system coincide with the streamlines of an incompressible inviscid fluid flow past the same inclusion (see Appendix C for proof). This analogy is very powerful, since flows past objects of many shapes and sizes have been established long ago.³⁵ The velocity field in the fluid maps to the chain stretch field, $\partial \mathbf{r} / \partial n$, in the brush. The complete set of analogous quantities in the brush and hydrodynamic systems are displayed in Table 1. For example, the unperturbed fluid kinetic energy density maps to the energy density of the brush without an inclusion:

$$\rho v_0^2 / 2 \rightarrow (3/2 a^5) (\partial \mathbf{r} / \partial n)^2 = P_A = 3h^2 / 2N^2 a^5 \quad (23)$$

where P_A is the energy density in the AG brush^{3–5} which in our language is the pressure. More generally, the change in fluid kinetic energy due to insertion of an object into the flow is analogous to the change in brush free energy due to insertion of this same object. Since the former is known in many cases, this allows the analogous energy change for the brush to be determined.

Note that it is easy to see why there can be no hydrodynamic analogy for the true end-annealed brush, for which the chain stretch field is not a single-valued function of the chain position \mathbf{r} since it depends also on which chain one selects at this position, according to the location of the chain end. That is, $\partial \mathbf{r} / \partial n$ depends on both \mathbf{r} and ρ . In the flow, of course, the fluid velocity field is a single-valued function of \mathbf{r} . Note the analogy in fact also applies to a third system: for type I superconductors, magnetic flux lines are expelled from a superconducting object (the complete Meissner effect³⁶). Placed in a constant external magnetic field, the flux lines follow the same paths as polymer chains in a brush–inclusion system.

Given a brush plus inclusion, the analogous hydrodynamic system involves a stationary inclusion in a moving fluid with far field velocity v_0 in the $+z$ direction, as shown in Figure 6. A technical issue is that literature flow problems are usually phrased as³⁵ objects moving with velocity v_0 in the $-z$ direction (see Figure 6) in a stationary fluid. To use the analogy, therefore, we must first translate from the stationary fluid system to the stationary inclusion system.

Consider first stationary fluid systems. The first row of Table 2 summarizes the fluid kinetic energy induced by various inclusion shapes, taken from the classic hydrodynamics text by Lamb.³⁵ For a sphere of volume V_p (Table 2, column b), the

Table 1. Analogous Quantities in the Brush, Hydrodynamics, and Magnetostatics Systems

Alexander–de Gennes brush	hydrodynamics	magnetostatics
polymer incompressibility	fluid incompressibility	$\nabla \cdot \mathbf{B} = 0$
chain paths, $\mathbf{r}(\rho, n)$	streamlines	B-field flux lines
chain stretching, $\partial \mathbf{r} / \partial n$	fluid velocity, v	B-field
$3/a^5$	fluid mass density, ρ	permittivity ⁻¹ , $1/\mu$
chain stretching energy, $(3/2 a^5) (\partial \mathbf{r} / \partial n)^2$	kinetic energy, $1/2 \rho v^2$	B-field energy, $B^2 / 2\mu$

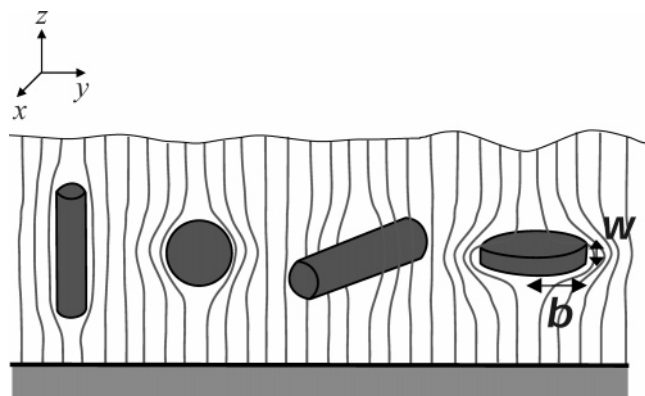


Figure 6. Inclusions of different shapes in an Alexander–de Gennes (AG) brush. Using the fact that polymers do not penetrate inclusions together with Kelvin’s minimum energy theorem,³⁵ an analogy can be shown with a hydrodynamical system: brush chain paths follow streamlines in the analogous hydrodynamic system. Hence, the kinetic energy of the fluid is analogous to the total chain stretching energy of the brush.



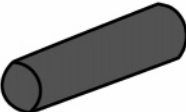
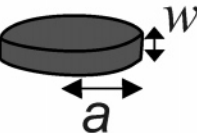
fluid kinetic energy is $(1/4)\rho v_0^2 V_p$, while the fluid mass displaced by the sphere is ρV_p ; hence, half of the displaced mass is added to the inertia of the sphere. In general, the fluid kinetic energy induced by the object depends on its shape. A long horizontal cylinder (Table 2, column c) induces twice the energy of the sphere of the same volume. Interestingly, the induced kinetic energy can vary by orders of magnitude for certain extreme shapes: a thin vertical cylinder (Table 2, column a) induces negligible energy because the object minimally interferes with the fluid motion, while a circular thin plate (Table 2, column d) creates a large disturbance regardless of its thickness, with an effect similar to that of a sphere of the same radius.

The translation from stationary fluid to stationary inclusion entails a velocity boost of the former system by v_0 in the $+z$ direction (see Figure 6); it is shown in Appendix D that this boost induces a fluid kinetic energy change equal to $\rho v_0^2 V_p$, regardless of shape. Thus, the inclusion-induced fluid energy change in the stationary inclusion system, shown in the second row of Table 2, is obtained by adding $\rho v_0^2 V_p$ to the first row of Table 2. Note that the energy expressions in the second row of Table 2 involve the unperturbed fluid kinetic energy density, $\rho v_0^2/2$. Replacing this with the unperturbed brush stretching energy density, P_A (see eq 23), gives our final results for the total inclusion-induced chain stretching energy of the brush (third row of Table 2).

C. Results: Energy Penalty Due to Inclusions of Various Shapes. The shape costing minimum energy is a thin vertical cylinder (Table 2, column a): the energy cost is $2P_A V_p$. The origin of this baseline energy is that in general the velocity boost (translating the stationary fluid to the stationary inclusion system) adds a shape-independent energy change $\rho v_0^2 V_p$ to the original shape-dependent kinetic energy. This change, $\rho v_0^2 V_p$, translates to a stretching energy change $2P_A V_p$ in the brush system. Since this additional energy penalty is independent of inclusion shape, $2P_A V_p$ is a lower bound for the energy required to insert an inclusion of volume V_p . The slender nature of the vertical cylinder in the very thin limit is such that there is no additional shape-dependent contribution in this case; lateral stretch is negligible, while vertical stretch due to polymer incompressibility costs $2P_A V_p$.

For other shapes, the total chain stretching energy exceeds this baseline of $2P_A V_p$. A sphere (Table 2, column b) costs total energy $(5/2)P_A V_p$, while a long horizontal cylinder (Table 2, column c) costs $3P_A V_p$. For these shapes the energy cost equals the baseline to within prefactors of order unity.

Table 2. Kinetic Energies in Brush Systems and the Analogous Fluid Systems for Different Shapes^a

	(a) 	(b) 	(c) 	(d) 
Fluid Kinetic Energy (Stationary Fluid System)	~ 0	$\frac{1}{2} \left(\frac{1}{2} \rho v_0^2 \right) V_p$	$\left(\frac{1}{2} \rho v_0^2 \right) V_p$	$\frac{8a}{3\pi w} \left(\frac{1}{2} \rho v_0^2 \right) V_p$
Fluid Kinetic Energy (Stationary Inclusion System)	$2 \left(\frac{1}{2} \rho v_0^2 \right) V_p$	$\frac{5}{2} \left(\frac{1}{2} \rho v_0^2 \right) V_p$	$3 \left(\frac{1}{2} \rho v_0^2 \right) V_p$	$\left(2 + \frac{8a}{3\pi w} \right) \left(\frac{1}{2} \rho v_0^2 \right) V_p$
ΔF^{inc} Alexander–de Gennes Brush	$2P_A V_p$	$\frac{5}{2} P_A V_p$	$3P_A V_p$	$\left(2 + \frac{8a}{3\pi w} \right) P_A V_p$
ΔF^{inc} for SCF Brush	$\Delta F = P(z) V_p$	$1 \leq \frac{\Delta F}{P(z) V_p} < \frac{5}{4}$	$1 \leq \frac{\Delta F}{P(z) V_p} < \frac{3}{2}$	$1 \leq \frac{\Delta F}{P(z) V_p} < \frac{4a}{3\pi w}$

^a First row: fluid kinetic energy induced by inclusion moving with speed v_0 in $-z$ direction (fluid stationary at infinity). Second row: induced fluid kinetic energy after “velocity boost”; fluid is then moving with speed v_0 in z direction while inclusion is stationary. Note the second row is obtained from the first row by adding the constant, $\rho v_0^2 V_p$. Third row: Alexander–de Gennes brush stretching energy induced by inclusion. This is obtained by replacing the unperturbed fluid energy density $(1/2)\rho v_0^2$ of the second row with the unperturbed brush stretching energy density P_A . Fourth row: lower and upper bounds for the free energy change due to an inclusion, ΔF^{inc} , in the correct end-annealed brush. The lower and upper bounds differ only by a prefactor of order unity with the exception of (d), the thin circular plate shape.

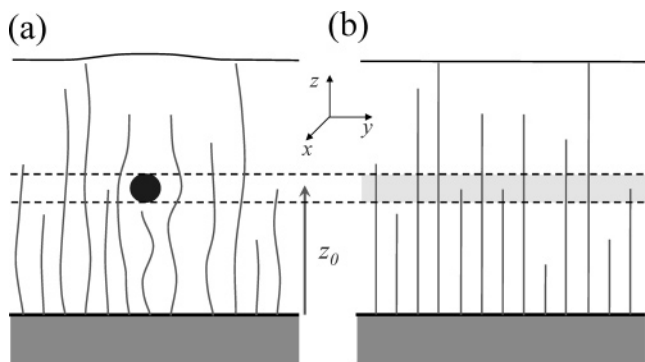


Figure 7. A single large inclusion of volume V_p distant z_0 from grafting surface. (b) The inclusion has been laterally uniformly smeared into a region of area A such that $\phi(z)A dz$ has the same volume as the particle in the height interval $(z, z + dz)$. In Appendix E we prove that the extra energy ΔF^{inc} due to the inclusion in (a) is always larger than the extra energy in (b). The latter is equal to $P(z_0)V_p$ for inclusions small compared to brush height.

Interestingly, for a circular thin plate (Table 2, column d) the induced energy is much larger than the baseline value. The shape-independent part, $2P_A V_p$, is negligible compared to the shape-dependent part $(8b/3\pi w)P_A V_p$ for plate thickness w much smaller than the plate radius, b . The thin plate generates a very large lateral chain stretch effect regardless of its thickness; hence, its effect is similar to that of a sphere of the same radius. Physically, this tells us that such a disk will tend to get rotated if kinetics permit.

VII. Large Inclusions in the End-Annealed Brush

In the previous section we calculated inclusion free energy penalties ΔF^{inc} in the approximate framework of the AG brush. In this section we address the true end-annealed brush. This is a rather difficult problem for large particles, which strongly perturb chain configurations. Our approach here is to establish lower and upper bounds on the free energy ΔF^{inc} . Much of our approach is motivated by our findings for the simpler AG brush.

A. Lower Bound for Free Energy. In Appendix E we prove that a lower bound for an inclusion of volume V_p at height z_0 in the true end-annealed brush is

$$\Delta F^{\text{inc}} \geq P(z_0)V_p \quad (24)$$

where $P(z)$ is the unperturbed pressure given by eq 1. This lower bound is the free energy one would get if one uniformly smeared out the particle laterally over a very large area A , so that $\phi(z)A dz$ has the same volume as the particle in the height interval $(z, z + dz)$ (see Figure 7). Here $\phi(z)$ is the volume fraction distribution in Figure 7b. For this distribution we can simply adopt our result from the small particle analysis treating nano-inclusions as a fluid, section IV, $\Delta F^{\text{inc}} = \int_0^h P(z)\phi(z) dz$ (eq 15). Physically this is sensible: if one allowed a particle to “dissolve” laterally (while constraining its height to be z_0), one would expect the equilibrium state to be a laterally symmetric one.

The requirement for this bound to be valid is that the particle size be small compared to brush height ($b \ll h$) such that the pressure variation in the region of the inclusion is small (see Appendix E).

B. Upper Bound for Free Energy. In Appendix F we prove that an upper bound for an inclusion of volume V_p at height z_0 in the true end-annealed brush is

$$\Delta F^{\text{inc}} \leq \beta(P(z_0)/2)V_p \quad (25)$$

where β is a shape-dependent constant (see Table 2, fourth row).

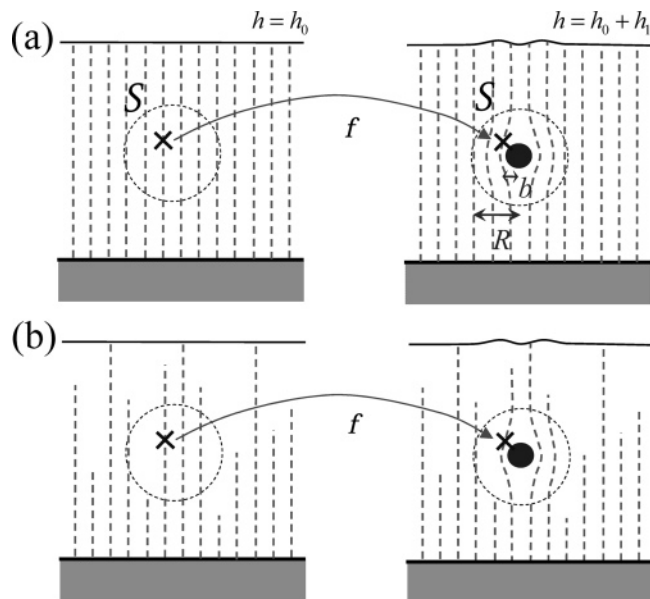


Figure 8. An Alexander–de Gennes brush before and after the addition of an inclusion. The brush configuration with the inclusion is constructed as follows. A sphere \mathcal{S} of radius R is imagined, such that chain paths outside of \mathcal{S} are vertical, while chain configurations within \mathcal{S} are determined by the condition that the energy must be a minimum in \mathcal{S} . This defines a mapping f from the unperturbed brush to the perturbed brush. (b) An end-annealed brush configuration is constructed similarly to (a), using the same mapping f . Note that outside \mathcal{S} the brush is unperturbed by the inclusion except for vertical translation.

The approach adopted in Appendix F starts from the observation that any brush configuration satisfying the polymer incompressibility constraint provides an upper bound to ΔF^{inc} , since the actual ΔF^{inc} corresponds to that configuration minimizing the brush–inclusion free energy. The challenge is to find a configuration whose free energy is close to the minimum value $P(z_0)V_p$. In Appendix F we determine such a “good” chain configuration. The chain paths are constructed through the following two steps: (i) A sphere \mathcal{S} of radius R enclosing the inclusion is imagined (see Figure 8); then we determine an AG brush configuration which minimizes the energy penalty within \mathcal{S} but leaves chain paths outside of the sphere as in the unperturbed AG brush. (ii) Adopting the monomer mapping function defined by (i), we construct chain paths for an inclusion in the end-annealed brush. This leads to the bound of eq 25.

C. Shape Dependence of Inclusion Energy. Our results for upper and lower bounds for energies of inclusions of different shapes are shown in Table 2 (fourth row). The lowest energy shape is a thin vertical cylinder (Table 2, column a) for which the upper and lower bounds coincide, giving us the precise result $P(z)V_p$. For most other shapes the bounds differ only by a prefactor of order unity: the energy penalty is between 1 and 1.25 times $P(z)V_p$ for a spherical inclusion, and between 1 and 1.5 times $P(z)V_p$ for a horizontal cylinder (see Table 2, columns b and c). For all of these shapes, therefore, we find the energy cost is close to the small particle result $P(z)V_p$ used to obtain the phase diagram of Figure 4. This phase diagram is thus qualitatively applicable to large particles as well ($b > \xi_{\text{blob}}$).

The thin circular plate shape is different (Table 2, column d). Here the lower bound $P(z)V_p$, which neglects lateral stretch, can be very different to the upper bound, $(4b/3\pi w)P(z)V_p$, where b and w are plate radius and thickness, respectively. In this case the bounds are not very useful, taken on their own. A simple estimate of ΔF^{inc} follows, using an argument similar to that of section VI. In the region within $\approx b$ of the inclusion, an excess pressure $\Delta P \approx P(z)$ is necessary to create the required lateral

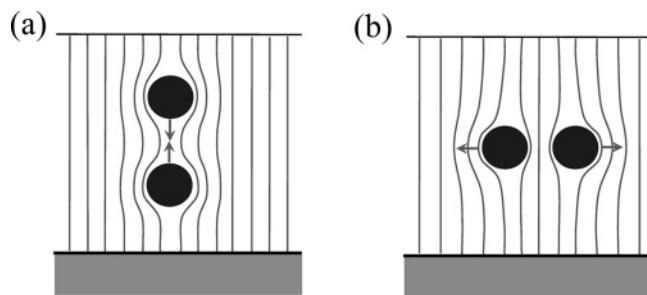


Figure 9. Effective brush-mediated interaction between nanoparticles is dipolar in the Alexander–de Gennes brush. (a) Vertically aligned particles attract. (b) Particles at the same horizontal level repel. Thus, horizontal plate-shaped aggregates tends to break up.

stretch. Thus, $\Delta F^{\text{inc}} \approx P(z)b^3 \approx (b/w)P(z)V_p$. We conjecture, therefore, that our upper bound is close to the true energy penalty. A brief report of these bounds has appeared in ref 8.

This section has considered single inclusions. Many-inclusion interactions are often important, for example, when mutually attractive inclusions aggregate. Applying the hydrodynamic analogy to a brush containing two inclusions, one sees the interaction is dipole-like: they attract when aligned vertically but repel when at the same horizontal level (see Figure 9). For the AG brush where the analogy is exact, this conclusion is directly applicable. However, in the SCF brush we only know bounds on the free energy, so solid conclusions are not possible. Nevertheless, the qualitative aspects of interparticle forces are likely to be the same as in AG brushes, since our results suggest a horizontal plate-shaped aggregate of several particles tends to break up into a vertical cylinder shape of the same volume, this having lower free energy.

Note that these effective interparticle interactions, however, may be overwhelmed by the buoyancy forces discussed previously: while the dipolar interaction energy between two particles separated by r is $\approx P(z)V_p^2/r^3$, the stretching energy is $P(z)V_p$. For separations large compared to particle size, therefore, the forces pushing particles toward the free brush surface will be much stronger than attractive or repulsive brush-induced forces.

VIII. Conclusions

We have studied the effect of inclusions on brush configurations and free energies which depends strongly on inclusion shape, size, and inclusion location in the brush. The free energy penalty ΔF^{inc} of introducing an inclusion determines how inclusions of size b distribute in the brush. For particles smaller than the typical fluctuation in monomer position, $b < \xi_{\text{blob}}$, we developed a self-consistent field (SCF) theory to show $\Delta F^{\text{inc}} = P(z)V_p$ per inclusion. In equilibrium this competes with entropy. Entropy dominates, giving a uniform distribution within the brush, for small inclusions, $b < b^*$ where $b^* \sim (N/h)^{2/3}$. Larger inclusions, $b > b^*$, are expelled to the brush surface, and the largest $b > b_{\text{max}}$ are expelled entirely, where $b_{\text{max}} \sim N^{1/4}$. This size-dependent phase behavior is summarized in the phase diagram of Figure 4.

The effect of big inclusions, $b > \xi_{\text{blob}}$, is qualitatively different because chain trajectories are forced to deviate strongly in the lateral directions (x, y in Figure 1). ΔF^{inc} then exceeds $k_B T$, and such a particle will ultimately be expelled. Since kinetics are often slow, however, an important issue is the value of $\Delta F^{\text{inc}}(z)$. We proved this has a lower bound $P(z)V_p$ (the small particle result), while we found upper bounds strongly dependent on shape. For most shapes we found $\Delta F^{\text{inc}}(z)$ equals $\beta P(z)V_p$, where β is a shape-dependent constant of order unity (see Table 2).

In particular, a thin vertical cylinder for which the upper and lower bounds coincide has energy penalty exactly $P(z)V_p$. For a given volume, then, vertical orientation and slender long shape gives the lowest free energy; thus, deformable inclusions will tend to suffer shape change in this direction before expulsion. For the circular plate shape (Table 2, column d) the bounds are not useful, and we conjecture this is the worst shape with highest energy.

In the phase diagram of Figure 4 the typical brush fluctuation scale ξ_{blob} is compared to the inclusion scales b^* and b_{max} . Now for an inclusion in the complete or partial mixing regimes, $b < b_{\text{max}}$, in most parts of the phase diagram the inclusion is then automatically smaller than ξ_{blob} so the phase diagram behavior, based on our small particle analysis, is a valid description. For bigger inclusions, $b > b_{\text{max}}$, the phase diagram predicts expulsion from the brush. But we know from our large inclusion analysis of section VII that the inclusion energy penalty is at least $P(z)V_p$; thus, this expulsion conclusion remains valid for these large particles. The one sector where the phase diagram is not self-consistent is the region $\xi_{\text{blob}} < b < b_{\text{max}}$; here we have only established free energy bounds. In most cases, however, the bounds yield energies equal to the small particle result to within prefactors of order unity. Overall, therefore, the phase diagram of Figure 4 is a reliable description regardless of particle size.

Let us now compare our conclusions to a few experiments and simulations. Thompson et al.¹² numerically studied lamellar phase A–B block copolymers mixed with A-like spherical nanoparticles. They solved SCF equations for the block copolymers together with density functional theory (DFT) for particles. For their system, we estimate $b^* = 0.09R_0$, where R_0 is the mean-square polymer end-to-end distance. They found particles of size $0.3R_0 = 3.3b^*$ resided near the center of the A layer, which in our language corresponds to the free surface of the brush. This is consistent with our prediction that large ($b > b^*$) particles are expelled from the brush layer. However, smaller particles of size $0.15R_0 = 1.7b^*$ preferred the region of the A layer near to the adjacent B layer. Since these are somewhat bigger than b^* , we conclude that energetic interactions (absent from our model) prevent expulsion for particles of this size.

Bockstaller et al.²⁴ studied poly(styrene-*b*-ethylene propylene) (PS–PEP) copolymers mixed with two different species of compatibilized nanoparticles. We estimate $b^* = 2.3$ nm for their system. One of the particle types, silica with mean radius 10.8 nm, resided at the center of the PEP layer. This is analogous to the free brush surface and consistent with our predictions for particle sizes above b^* . On the other hand, gold particles of mean radius 1.75 nm, smaller than b^* , were observed to occupy the PS–PEP dividing surface, which corresponds to the brush grafting surface. Our prediction is that they should distribute fairly uniformly within one of the two layers. We speculate that the energy interactions between nanoparticles and the two copolymer blocks, which are of course beyond our simple particle–brush analysis, may result in particles preferring the dividing surface provided particle size is not so great that its stretching energy penalty is severe. We hope that future theoretical and experimental studies of brush and copolymer systems will help to clarify the competition between these entropic and energetic effects.

Acknowledgment. This work was supported primarily by the MRSEC Program of the National Science Foundation under Award Number DMR-0213574 at Columbia University. Acknowledgment is also made to the donors of the American

Chemical Society Petroleum Research Fund for partial support of this research.

Appendix A. Calculation of Chain End Distribution

In the end-annealed SCF brush, a specific chain end distribution $g(\rho)$ minimizes the free energy while maintaining incompressibility of the system. In this appendix $g(\rho)$ is derived. The inclusion volume fraction at position z is $\phi(z)$, so the monomer volume fraction is $1 - \phi(z)$, which must equal the sum of monomer density contributions from all chains passing through z whose ends ρ lie between z and h :

$$\int_z^h d\rho \frac{g(\rho)}{|\partial z(\rho, n)/\partial n|} = \frac{1 - \phi(z)}{a^3} \quad (\text{A1})$$

The meaning of the stretch function, $\partial z(\rho, n)/\partial n$, is the distance between consecutive monomers at position z , so its inverse is the monomer density contribution of the given chain.

We seek the function $g(\rho)$ that satisfies this equation for all z . Using eq 3 for the chain stretch $\partial z(\rho, n)/\partial n$, this gives

$$\int_z^h d\rho \frac{g(\rho)}{\sqrt{\rho^2 - z^2}} = f(z) \quad (\text{A2})$$

where $f(z) = \pi(1 - \phi(z))/2Na^3$. Multiplying both sides by $z/\sqrt{z^2 - w^2}$ and integrating over z , we have

$$\int_w^h dz \int_z^h d\rho \frac{zg(\rho)}{\sqrt{\rho^2 - z^2}\sqrt{z^2 - w^2}} = \int_w^h dz \frac{zf(z)}{\sqrt{z^2 - w^2}} \quad (\text{A3})$$

The term on the left can be simplified by changing the order of integration to $\int_w^h d\rho \int_\rho^h dz$. Then the inner integral, $\int_\rho^h dz \frac{z}{\sqrt{z^2 - w^2}\sqrt{z^2 - \rho^2}}$, equals $\pi/2$ independent of w and ρ . Then, by integrating the term on the right by parts, we have

$$\int_w^h d\rho g(\rho) = \frac{2}{\pi} \left(\sqrt{h^2 - w^2} f(h) - \int_w^h dz \sqrt{z^2 - w^2} f'(z) \right) \quad (\text{A4})$$

Finally, differentiating both sides with respect to w gives

$$g(\rho) = \frac{2\rho}{\pi} \left(\frac{f(h)}{\sqrt{h^2 - \rho^2}} - \int_\rho^h dz \frac{f'(z)}{\sqrt{z^2 - \rho^2}} \right) \quad (\text{A5})$$

This gives eq 12 in the main text after inserting the explicit form of f .

Appendix B. Stretching Energy Penalty Due to Inclusions

A great advantage of the SCF approach is that the full brush configuration can be explicitly obtained. This remains true when inclusions are present, provided the inclusion density distribution has x and y directional symmetry (see Figure 1). In this appendix we calculate how the brush configuration is modified due to an inclusion density profile $\phi(z)$. We then obtain the exact chain stretching energy.

The one-dimensional version of the total brush free energy, eq 9, is

$$F^{\text{brush}} = \frac{3}{2a^2} \int_0^h d\rho g(\rho) \int_0^N dn \left(\frac{\partial z(\rho, n)}{\partial n} \right)^2 - \eta \left(\int_0^h d\rho g(\rho) - \sigma \right) + \int_0^h dz P(z) a^3 \times \left(\int_z^h d\rho \frac{g(\rho)}{|\partial z(\rho, n)/\partial n|} - \frac{1 - \phi(z)}{a^3} \right) \quad (\text{B1})$$

As in eq 9, the first term is the chain stretching energy while the second term represents the constraint that chain grafting density of this brush is σ . The last term is due to the space-filling condition, eq A1. In this 1D expression, the pressure field $P(z)$ depends only on z and the other Lagrange multiplier, η , is a scalar.

The last term of eq B1 can be simplified by changing the order of integration, $\int_0^h d\rho \int_0^N dn$. Then, changing the integration variable from z to n , the first part of the last term becomes

$$\int_0^h d\rho \int_0^N dn P(z) a^3 \frac{g(\rho)}{|\partial z(\rho, n)/\partial n|} = \int_0^h d\rho g(\rho) \int_0^N dn P(z(\rho, n)) a^3 \quad (\text{B2})$$

Minimizing the total free energy F^{brush} with respect to the function $g(\rho)$, each chain path must satisfy the following condition:

$$\frac{3}{2a^2} \int_0^N dn \left(\frac{\partial z(\rho, n)}{\partial n} \right)^2 + \int_0^N dn P(z(\rho, n)) a^3 = \eta = P_0 Na^3 \quad (\text{B3})$$

The first term of the left-hand side is the stretching energy of a given chain whose end is at ρ , while the second term is the work which must be done against the pressure to insert the chain into the brush. Thus, the physical meaning of this equation is that, regardless of chain end position, all chains have the same chemical potential η , and hence the symmetry between chains is broken such that chain ends can lie anywhere in the brush. The explicit value of η is obtained by considering a chain at $\rho = 0$; such a chain has zero stretching energy and has pressure energy $P_0 Na^3$.

Using eq B3, the total stretching energy is

$$F^{\text{stretch}} = \frac{3}{2a^2} \int_0^h d\rho g(\rho) \int_0^N dn \left(\frac{\partial z(\rho, n)}{\partial n} \right)^2 = \int_0^h d\rho g(\rho) \int_0^N dn (P_0 - P(z(\rho, n))) a^3 \quad (\text{B4})$$

This can be readily evaluated from the pressure field, without explicitly using the complex chain end distribution function $g(\rho)$, as follows. Changing integration variable from n to z and reversing the order of integration, we have

$$F^{\text{stretch}} = \int_0^h dz (P_0 - P(z)) \int_z^h d\rho \frac{g(\rho) a^3}{|\partial z(\rho, n)/\partial n|} = \int_0^h dz (P_0 - P(z)) (1 - \phi(z)) \quad (\text{B5})$$

where the ρ integral equals $(1 - \phi(z))$, the monomer density at position z (see eq A1).

Using the quadratic pressure profile, eq 1, this is rewritten

$$F^{\text{stretch}} = \int_0^h dz \left(P_0 \frac{z^2}{h^2} - P_0 \phi(z) + P(z) \phi(z) \right) = \frac{1}{3} P_0 h - P_0 \bar{\phi} h + \int_0^h dz P(z) \phi(z) \quad (\text{B6})$$

The brush height with inclusions is $h = h_0/(1 - \bar{\phi})$, increased from the pure brush value, h_0 . Thus, the sum of the first two terms is $(\pi^2 h_0^3 / 8Na^5) (1 - \bar{\phi}) / (1 - \bar{\phi})^3$. Taylor expanding with respect to $\bar{\phi}$, its dependence on $\bar{\phi}$ vanishes to first order. Thus, if the mean inclusion density is small, $\bar{\phi} \ll 1$, the change of chain stretching energy is

$$\Delta F^{\text{inc}} = \int_0^h dz P(z) \phi(z) \quad (\text{B7})$$

Appendix C. Analogy between Brushes and Hydrodynamics

In this appendix, following Williams and Pincus,³⁴ we show how the formal solution of the Alexander–de Gennes (AG) brush is analogous to a specific hydrodynamical system. In the AG brush, chain end positions are fixed at the free surface. Thus, the brush chain stretch $\mathbf{u} = \partial \mathbf{r} / \partial n$ is a well-defined vector field. The total stretching energy is the sum of contributions from each position \mathbf{r} , where the stretching energy is $(3/2a^2)(\partial \mathbf{r} / \partial n)^2$ per monomer:

$$F^{\text{stretch}} = \frac{3}{2a^2} \int \frac{d\mathbf{r}}{a^3} \left(\frac{\partial \mathbf{r}}{\partial n} \right)^2 = \frac{3}{2a^5} \int \mathbf{u}^2 d\mathbf{r} \quad (\text{C1})$$

We seek the chain stretch field \mathbf{u} minimizing F^{stretch} . Now Kelvin's Minimum Energy Theorem (see ref 35) states that \mathbf{u} must be curl-free to minimize the energy; hence, \mathbf{u} is the negative gradient of a "chain stretch potential" $\psi(\mathbf{r})$, $\mathbf{u} = -\nabla \psi(\mathbf{r})$. At the same time, from the incompressible nature of the dry polymer brush, the chain stretch field must satisfy $\nabla \cdot \mathbf{u} = 0$. Thus, $\psi(\mathbf{r})$ is a solution of the Laplace equation, $\nabla^2 \psi(\mathbf{r}) = 0$.

This solution is well determined if the boundary conditions are given. For the brush–inclusion system the boundary conditions are that the chain stretch field \mathbf{u} converges to a constant, \mathbf{u}_0 , far from the inclusions, while at the surface of all inclusions the stretch field \mathbf{u} must be parallel to the inclusion surface.

We can see that this brush–inclusion system is analogous to a hydrodynamic system in which an incompressible inviscid fluid flow with constant velocity \mathbf{u}_0 is perturbed by inclusions, as follows. The velocity potential of the hydrodynamical system satisfies Laplace's equation³⁵ with slip boundary condition at inclusion surfaces. Thus, because of the uniqueness of solutions, the fluid velocity field and chain stretch field are identical. This proves the analogy. Equation C1 indicates that the fluid mass density has the analogy $\rho \rightarrow 3/a^5$.

Note that the magnetic potential of a magnetostatic system also follows Laplace's equation. The slip boundary condition of a brush–inclusion system is the same as that for a type I superconductor exhibiting the complete Meissner effect.³⁶ Thus, a type I superconductor in constant external magnetic field is a second analogy. Table 1 lists the analogous quantities in these three systems.

Appendix D. Fluid Kinetic Energy Change Due to Velocity Boost

In this appendix we calculate the change in kinetic energy when a conversion is made from a "fluid–stationary" to an "inclusion–stationary" system. Assuming an inclusion of volume V_p is moving in the stationary fluid of volume V with velocity v_0 in the $-z$ direction (see Figure 6), the fluid streamlines and kinetic energy depend on the inclusion geometry only, independent of inclusion mass. For convenience, we set the inclusion mass density to ρ , equal to the fluid density, so the center of mass of the system is stationary. The total kinetic energy is the fluid kinetic energy induced by the inclusion, say T_f , plus the inclusion kinetic energy, $(\rho v_0^2/2)V_p$. Now we implement the frame boost by adding velocity v_0 to all components of the system. It is well-known that the relation between the kinetic energy in the center of mass frame, T_{CM} , and the kinetic energy in the new frame, T_{total} , is $T_{\text{total}} = T_{\text{CM}} +$

$(1/2)M_{\text{total}}v_0^2$, where M_{total} is the total mass of the system. Thus, $T_{\text{total}} = T_f + (\rho v_0^2/2)V_p + (\rho v_0^2/2)(V + V_p)$. Subtracting the original fluid kinetic energy $(\rho v_0^2/2)V$ from T_{total} , the change of kinetic energy due to the inclusion is

$$\Delta T = T_f + \rho v_0^2 V_p \quad (\text{D1})$$

In the new frame, the inclusion is stationary so this kinetic energy is purely due to fluid movement. Hence, the density of the inclusion (set here to ρ) is irrelevant to the result. Thus, in converting from a fluid–stationary to an inclusion–stationary system, the velocity boost adds a constant kinetic energy $\rho v_0^2 V_p$. The energy changes for the four shapes are listed in the third row of Table 2. The quantity $\rho v_0^2 V_p$ translates to $2P_A V_p$ in the analogous brush–inclusion system; hence, an energy penalty $2P_A V_p$ is inevitable, regardless of inclusion shape. This is the lower bound of the energy penalty to insert an inclusion of volume V_p into the brush.

Appendix E. Lower Bound for Free Energy Due to Large Inclusions

In this appendix we show the lower bound for the free energy penalty due to a large inclusion of volume V_p at height z_0 is $P(z_0)V_p$. We will prove that the free energy penalty due to one inclusion (Figure 7a) always exceeds the penalty in the brush situation of Figure 7b, where the inclusion has been laterally uniformly smeared into a region of area A so that $\phi(z)A dz$ has the same volume as the particle in the height interval $(z, z + dz)$. Here $\phi(z)$ is the volume fraction distribution in Figure 7b. For large A , this is a laterally symmetric situation for which the exact energy penalty $P(z_0)V_p$ is known from our small inclusion analysis, section IV.

The end distribution function $g(\rho)$ and chain paths $\mathbf{r}(\rho, n)$ in Figure 7a assume the values minimizing F^{brush} . Let us define the chain stretch at height z of the chain whose end is at position ρ to be $\mathbf{u}(\rho, z) \equiv \partial \mathbf{r}(\rho, n) / \partial n$. Note the functions $g(\rho)$ and $\mathbf{u}(\rho, z)$ completely define the brush configuration. Interestingly, we can make the following lateral average of these functions representing a physically realizable brush configuration for the laterally symmetric situation of Figure 7b:

$$g_{\text{avg}}(\rho_z) \equiv \int g(\rho) d\rho_{\perp}, \quad \frac{g_{\text{avg}}(\rho_z)}{u_{\text{avg}}(\rho_z, z)} \equiv \int \frac{g(\rho)}{u_z(\rho, z)} d\rho_{\perp} \quad (\text{E1})$$

To show $g_{\text{avg}}(\rho_z)$ and $u_{\text{avg}}(\rho_z, z)$ indeed represent a valid symmetric brush configuration, we must check the following conditions are satisfied: (i) $g_{\text{avg}}(\rho_z)$ gives the correct total number of chains; (ii) the local monomer density at height z equals $1 - \phi(z)$; (iii) the stretch field is such that every chain has length N .

From the definition of $g_{\text{avg}}(\rho_z)$, $\int g_{\text{avg}}(\rho_z) d\rho_z = \int g(\rho) d\rho$; thus, the total chain number is correct (note that $g_{\text{avg}}(\rho_z)/A$ is the chain end density per unit volume). Similarly, (ii) can be proved by showing the polymer density at height z is the same in the two situations of Figure 7a,b: $\int (g_{\text{avg}}(\rho_z)/u_{\text{avg}}(\rho_z, z)) d\rho_z = \int (g(\rho)/u_z(\rho, z)) d\rho = 1 - \phi(z)$. To show (iii), we express number of monomers in a chain whose end is at $u_{\text{avg}}(\rho_z, z)$ as follows:

$$\int dz \frac{1}{u_{\text{avg}}(\rho_z, z)} = \int dz \frac{1}{g_{\text{avg}}(\rho_z)} \int d\rho_{\perp} \frac{g(\rho)}{u_z(\rho, z)} = \int d\rho_{\perp} \frac{g(\rho)}{g_{\text{avg}}(\rho_z)} \int dz \frac{1}{u_z(\rho, z)} \quad (\text{E2})$$

The last integral, $\int dz (1/u_z(\rho, z))$, equals N for any ρ because this

represents the number of monomers in a chain in Figure 7a. Then the integral with respect to ρ_\perp equals unity from definition of $g_{\text{avg}}(\rho_z)$ (eq E1); thus, every chain has N monomers. This completes the proof that $g_{\text{avg}}(\rho_z)$ and $u_{\text{avg}}(\rho_z, z)$ represent a realizable chain configuration for the problem with symmetry (Figure 7b).

The total energy F^{brush} of Figure 7a can be written

$$F^{\text{brush}} = \frac{3}{2a^2} \int d\rho \, g(\rho) \int \frac{dz}{u_z(\rho, z)} \mathbf{u}^2(\rho, z) \quad (\text{E3})$$

where $dz/u_z(\rho, z) = dn$. Let us now show F^{brush} exceeds $F_{\text{avg}}^{\text{brush}}$, the energy of our just constructed symmetric configuration defined by $g_{\text{avg}}(\rho_z)$, $u_{\text{avg}}(\rho_z, z)$. First, we use the inequality $u_z(\rho, z) < \mathbf{u}^2(\rho, z)/u_z(\rho, z)$ in eq E3 to obtain

$$F^{\text{brush}} > \frac{3}{2a^2} \int dz \int d\rho_z \int d\rho_\perp g(\rho) u_z(\rho, z) \quad (\text{E4})$$

Then, using the Cauchy–Schwarz integral inequality, it is straightforward to show the last integral, $\int d\rho_\perp g(\rho) u_z(\rho, z)$, exceeds $g_{\text{avg}}(\rho_z) u_{\text{avg}}(\rho_z, z)$. Since $F_{\text{avg}}^{\text{brush}} \equiv \int dz \int d\rho_z g_{\text{avg}}(\rho_z) u_{\text{avg}}(\rho_z, z)$, this proves $F^{\text{brush}} > F_{\text{avg}}^{\text{brush}}$.

Note that $g_{\text{avg}}(\rho_z)$, $u_{\text{avg}}(\rho_z, z)$ is not necessarily the self-consistent minimum energy configuration corresponding to Figure 7b. In section IV, we showed the energy change on adding the inclusion field for this case is $A \int dz P(z) \phi(z)$. Since this is the minimum free energy situation, when added to the unperturbed brush stretching energy, this must be less than $F_{\text{avg}}^{\text{brush}}$. It follows that the energy penalty due to the inclusion obeys the inequality

$$\Delta F^{\text{inc}} > A \int dz P(z) \phi(z) = P(z_0) V_p \quad (\text{E5})$$

where the last equation requires particle size b much less than the brush height h , so the pressure variation over the region occupied by the particle is small.

Appendix F. Upper Bound for Free Energy Due to Large Inclusions

In this appendix we calculate the upper bound for the free energy penalty due to a large inclusion of volume V_p at height z_0 . Consider first a nonequilibrium configuration of the AG brush containing one inclusion of size b , as in Figure 8a, which we will construct so as to be a good approximation to the true equilibrium configuration of the AG brush plus inclusion. This configuration respects incompressibility but does not minimize the free energy. Introducing an imaginary sphere \mathcal{J} of radius R centered on the particle, this configuration is constructed as follows: (i) chain paths outside the sphere are *unperturbed* by the inclusion (i.e., chains follow vertical lines as in the unperturbed AG brush); (ii) inside \mathcal{J} , the configuration is that minimizing the free energy in \mathcal{J} subject to the incompressibility constraint.

Thus, the sphere contains a subregion of a minimum free energy AG brush, albeit with unusual boundary conditions on the sphere surface. What are these boundary conditions? It is straightforward to show that incompressibility forces the radial component of the stretch field $\partial \mathbf{r} / \partial n$ to be continuous across the surface of \mathcal{J} . Since $\partial \mathbf{r} / \partial n = -(h_0/N) \hat{\mathbf{z}}$ is known outside \mathcal{J} , the radial component is thus given for all points on \mathcal{J} . Following the prescription of the hydrodynamic analogy, the minimum free energy configuration within \mathcal{J} is obtained by solving Laplace's equation for the "chain stretch potential" ψ (defined by $\partial \mathbf{r} / \partial n = -\nabla \psi$) as explained in Appendix C. It is well-known

that Laplace's equation has a unique solution if the normal component of its gradient is specified everywhere on the boundary. Hence, the chain configuration within \mathcal{J} is uniquely determined by our construction.

Note the number of monomers along a given chain trajectory in \mathcal{J} may differ from the value before the inclusion was introduced (since the stretch field is changed); this changes the number of monomers along the same trajectory continued outside \mathcal{J} and induces an increase or decrease in brush height relative to the unperturbed brush (see Figure 8a). This is the "bump" on the brush surface due to the embedded inclusion.

Later in this appendix we will choose the sphere radius R to be large compared to particle size b , so the constructed configuration's free energy is a good approximation to that of the AG brush plus nanoinclusion system. For example, the energy of a spherical inclusion in the constructed solution, $(5/2)P_A V_p (1 + O(V_p/R^3))$, equals the exact result (Table 2, column b) plus a small correction.³⁵

Let us now turn to the end-annealed brush plus inclusion. We construct a configuration (Figure 8b) similarly to our AG brush prescription above: outside \mathcal{J} the brush is unperturbed by the inclusion (except for changes in the numbers of monomers along trajectories and a consequent height perturbation); inside \mathcal{J} , we use the same spatial mapping of monomers as that used for the AG brush, above. Thus, a monomer originally at \mathbf{r}_0 in the unperturbed brush is mapped to a location $\mathbf{f}(\mathbf{r}_0)$ in the constructed brush, where $\mathbf{r}_0 \rightarrow \mathbf{f}(\mathbf{r}_0)$ is the mapping we defined above for the AG brush. Note that the mapping $\mathbf{r}_0 \rightarrow \mathbf{f}(\mathbf{r}_0)$ is volume preserving by construction. Thus, we have constructed a space-filling configuration of the end-annealed brush with inclusion (see Figure 8b).

We will now use the constructed end-annealed brush configuration to obtain an upper free energy bound valid in the limit of particle size much less than brush height, $b \ll h$. The argument hinges on the fact that due to the linearity of the hydrodynamic analogue³⁵ the mapping $\mathbf{r}_0 \rightarrow \mathbf{f}(\mathbf{r}_0)$ depends only on the geometry of the inclusion, independent of the unperturbed stretch $|\partial \mathbf{r}_0(n)/\partial n|$. In the hydrodynamics language increasing the fluid velocity without inclusion does not change the streamlines with the inclusion; in the brush language, increasing the uniform stretch $|\partial \mathbf{r}_0(n)/\partial n|$ of the unperturbed brush by some constant factor α increases the stretch field in the perturbed brush by α everywhere but does not change the chain trajectories. Thus, a chain segment at \mathbf{r}_0 belonging to a chain whose end is at ρ_0 is stretched by the same factor $\lambda(\mathbf{r}_0)$ regardless of how stretched it was initially and independent of ρ_0 :

$$\frac{|\partial \mathbf{f}(\mathbf{r}_0(\rho_0, n))/\partial n|}{|\partial \mathbf{r}_0(\rho_0, n)/\partial n|} \equiv \lambda(\mathbf{r}_0) \quad (\text{F1})$$

Now we choose the sphere \mathcal{J} to be small compared to brush height, $R \ll h$, so the unperturbed pressure in the end-annealed brush is approximately constant throughout \mathcal{J} , equal to $P(z)$ for an inclusion at z (see eq 1). (Recall that we simultaneously choose $R \gg b$; thus, our method assumes inclusion size is much less than brush height.)

Using the exact result that the energy density of the end-annealed brush is $P(z)/2$ (we prove this in Appendix G), it follows that the energy density throughout \mathcal{J} is approximately constant in the unperturbed brush. Since energies scale as the square of chain stretch, eq F1 thus tells us that the ratio of the brush energies in \mathcal{J} before and after the mapping $\mathbf{r}_0 \rightarrow \mathbf{f}(\mathbf{r}_0)$ is the same for both the AG and end-annealed brush constructions. Since the unperturbed AG brush has energy density P_A , we have

$$\frac{\Delta F_{AG}^{inc}}{P_A V_S} = \frac{\Delta F_{EA}^{inc}}{(P(z)/2) V_S} \quad (F2)$$

where subscripts AG and EA denote the constructed configurations of Figures 8a and 8b, respectively, and V_S is the volume of \mathcal{J} . We used the fact that the energy changes outside \mathcal{J} vanish.

Recall that for large V_S/V_p the constructed AG brush energy change ΔF_{AG}^{inc} is a good approximation to the true energy change for the AG brush calculated in section VI. Hence $\Delta F_{AG}^{inc} \approx \beta P_A V_p$ where β is shape-dependent (see Table 2, third row) and from eq F2

$$\Delta F_{EA}^{inc} \approx \beta (P(z)/2) V_p \quad (F3)$$

This is our final result: an upper bound ΔF_{EA}^{inc} is obtained by simply taking our already established results for the AG brush in the third row of Table 2 and replacing $P_A \rightarrow P(z)/2$.

Appendix G. Local Brush Stretching Energy Density

For the unperturbed SCF brush, the stretch of a chain $\partial z(\rho, n)/\partial n$ is a function of both ρ and z . By averaging contributions from all chains passing through z , we calculate below the mean stretching energy density $F^{\text{stretch}}(z)$. All chains with end position ρ greater than z contribute, but with different contributions to the monomer density according to eq A1 (at $\phi(z) \equiv 0$). Thus

$$F^{\text{stretch}}(z) = \int_z^h d\rho \frac{g(\rho)}{|\partial z(\rho, n)/\partial n|} \frac{3}{2a^2} \left(\frac{\partial z(\rho, n)}{\partial n} \right)^2 \quad (G1)$$

Using eqs 1 and 3, this gives

$$F^{\text{stretch}}(z) = \frac{2P_0}{\pi h^2} \int_z^h d\rho \frac{\rho \sqrt{\rho^2 - z^2}}{\sqrt{h^2 - \rho^2}} \quad (G2)$$

Evaluating the integral, we have

$$F^{\text{stretch}}(z) = \frac{P_0}{2h^2} (h^2 - z^2) = \frac{1}{2} P(z) \quad (G3)$$

Interestingly, the mean stretching energy density at a given height z is always one-half of the pressure value of the

unperturbed brush. This allows us to calculate the energy penalty of our trial configuration in Appendix F.

References and Notes

- (1) Semenov, A. N. *Sov. Phys. JETP* **1985**, *61*, 733–742.
- (2) Likhtman, A. E.; Semenov, A. N. *Macromolecules* **1994**, *27*, 3103–3106.
- (3) Alexander, S. *J. Phys. (Paris)* **1977**, *38*, 983–987.
- (4) de Gennes, P. G. *Macromolecules* **1980**, *13*, 1069–1075.
- (5) Rabin, Y.; Alexander, S. *Europhys. Lett.* **1990**, *13*, 49–54.
- (6) Milner, S. T.; Witten, T. A.; Cates, M. E. *Macromolecules* **1988**, *21*, 2610–2619.
- (7) Milner, S. T. *Science* **1991**, *251*, 905–914.
- (8) Kim, J. U.; O'Shaughnessy, B. *Phys. Rev. Lett.* **2002**, *89*, 238301.
- (9) Solis, F. J. *Macromolecules* **1996**, *29*, 4060–4065.
- (10) Solis, F. J.; Tang, H. *Macromolecules* **1996**, *29*, 7953–7959.
- (11) Huh, J.; Ginzburg, V. V.; Balazs, A. C. *Macromolecules* **2000**, *33*, 8085–8096.
- (12) Thompson, R. B.; Ginzburg, V. V.; Matsen, M. W.; Balazs, A. C. *Science* **2001**, *292*, 2469–2472.
- (13) Lee, J.-Y.; Thompson, R. B.; Jasnow, D.; Balazs, A. C. *Phys. Rev. Lett.* **2002**, *89*, 155503.
- (14) Lee, J. Y.; Thompson, R. B.; Jasnow, D.; Balazs, A. C. *Faraday Discuss.* **2003**, *123*, 121–131.
- (15) Bhat, R. R.; Genzer, J.; Chaney, B. N.; Sugg, H. W.; Liebmann-Vinson, A. *Nanotechnology* **2003**, *14*, 1145–1152.
- (16) Bhat, R. R.; Tomlinson, M. R.; Genzer, J. *Macromol. Rapid Commun.* **2004**, *25*, 270–274.
- (17) Halperin, A. *Langmuir* **1999**, *15*, 2525–2533.
- (18) Sofia, S. J.; Premnath, V.; Merrill, E. W. *Macromolecules* **1998**, *31*, 5059–5070.
- (19) McPherson, T.; Kidane, A.; Szleifer, I.; Park, K. *Langmuir* **1998**, *14*, 176–186.
- (20) Satulovsky, J.; Carignano, M. A.; Szleifer, I. *Proc. Natl. Acad. Sci. U.S.A.* **2000**, *97*, 9037–9041.
- (21) Ball, R. C.; Marko, J. F.; Milner, S. T.; Witten, T. A. *Macromolecules* **1991**, *24*, 693–703.
- (22) Bockstaller, M.; Kolb, R.; Thomas, E. L. *Adv. Mater.* **2001**, *13*, 1783–1786.
- (23) Bockstaller, M. R.; Thomas, E. L. *J. Phys. Chem. B* **2003**, *107*, 10017–10024.
- (24) Bockstaller, M. R.; Lapetnikov, Y.; Margel, S.; Thomas, E. L. *J. Am. Chem. Soc.* **2003**, *125*, 5276–5277.
- (25) Likhtman, A. E.; Semenov, A. N. *Europhys. Lett.* **2000**, *51*, 307–313.
- (26) Netz, R. R.; Schick, M. *Europhys. Lett.* **1997**, *38*, 37–42.
- (27) Marko, J. F.; Witten, T. A. *Phys. Rev. Lett.* **1991**, *66*, 1541–1544.
- (28) Witten, T. A.; Leibler, L.; Pincus, P. A. *Macromolecules* **1990**, *23*, 824–829.
- (29) Semenov, A. N. *Macromolecules* **1992**, *25*, 4967–4977.
- (30) Semenov, A. N. *Macromolecules* **1993**, *26*, 2273–2281.
- (31) Likhtman, A. E.; Semenov, A. N. *Macromolecules* **1997**, *30*, 7273–7278.
- (32) Floudas, G.; Hadjichristidis, N.; Stamm, M.; Likhtman, A. E.; Semenov, A. N. *J. Chem. Phys.* **1997**, *106*, 3318–3328.
- (33) Xi, H.; Milner, S. T. *Macromolecules* **1996**, *29*, 2404–2411.
- (34) Williams, D. R. M.; Pincus, P. A. *Europhys. Lett.* **1993**, *24*, 29–34.
- (35) Lamb, H. *Hydrodynamics*; Dover Publications: New York, 1945.
- (36) Kittel, C. *Introduction to Solid State Physics*; Wiley: New York, 1996.

MA0508171